J|A|C|S
ARTICLES
Published on Web 07/07/2005

Photoinduced Charge Transfer Processes along Triarylamine Redox Cascades

Christoph Lambert,*,† Jürgen Schelter,† Torsten Fiebig,*,‡ Daniela Mank,‡ and Anton Trifonov‡

Contribution from the Institut für Organische Chemie, Bayerische Julius-Maximilians-Universität Würzburg, Am Hubland, D-97074 Würzburg, Germany, and Boston College, Department of Chemistry, Eugene F. Merkert Chemistry Center, 2609 Beacon Street, Chestnut Hill, MA 02467

Received February 23, 2005; E-mail: lambert@chemie.uni-wuerzburg.de; Fiebig@bc.edu

Abstract: In this paper, we describe the synthesis and photophysical properties of a series of acridine−triarylamine redox cascades. These cascades were designed in order to promote photoinduced hole transfer from an acridine fluorophore into an adjacent triarylamine. The excited dipolar state then injects a hole into the triarylamine redox cascade. Subsequently, the hole migrates along the redox gradient which was tuned by the substituents attached to the triarylamine redox centers. The rate of hole migration was determined by fluorescence lifetime measurements and is in the ns regime and depends strongly on the solvent polarity. The photophysical processes were also investigated by femtosecond broadband pump−probe spectroscopy. Our studies reveal different dynamic processes in the cascades depending on the solvent polarity, e.g., direct charge separation after photoexcitation vs a two step hole transfer mechanism.

Introduction

Electron transfer (ET) or, more precisely, hole transfer (HT) processes in triarylamine based systems have thoroughly been investigated in the past.[1−4] Owing to the relatively simple synthetic accessibility and the stability of oxidized triarylamines these units are widely used as hole transport components in optoelectronic devices.[5−10] But also on a molecular level, triarylamines have attracted considerable interest: the triarylamine group was used as the charge bearing unit in organic mixed valence compounds for intramolecular ET studies[1−4,11−15] as well as in organic high spin systems for organic ferromagnets.[16−26] One-dimensional systems with two triarylamine groups have been investigated but also cascades with many triarylamines in a row[27−29] up to polymers[11,30] and dendrimers.[31−36] In the present study, we will focus on triarylamine cascades in which a hole can be transferred along a redox gradient. The redox centers of these cascades are built up from triarylamines connected by acetylene spacers. The hole is injected in the cascade by photoinduced electron transfer (PET) of an excited acridine chromophore. Triarylamines were used as redox centers for the above-mentioned reasons but also

† Bayerische Julius-Maximilians-Universität Würzburg.
‡ Boston College.

(1) Lambert, C.; Nöll, G.; Schelter, J. *Nat. Mater.* **2002**, *1*, 69−73.
(2) Lambert, C.; Nöll, G. *Chem. Eur. J.* **2002**, *8*, 3467−3477.
(3) Lambert, C.; Nöll, G. *J. Am. Chem. Soc.* **1999**, *121*, 8434−8442.
(4) Lambert, C.; Amthor, S.; Schelter, J. *J. Phys. Chem. A* **2004**, *108*, 6474−6486.
(5) Zhao, H. T. C.; Thayumanavan, S. *Tetrahedron Lett.* **2001**, *42*, 4421−4424.
(6) Fujikawa, H.; Tokito, S.; Taga, Y. *Synth. Met.* **1999**, *91*, 161−162.
(7) Thayumanavan, S.; Barlow, S.; Marder, S. R. *Chem. Mater.* **1997**, *9*, 3231−3235.
(8) Koene, B. E.; Loy, D. E.; Thompson, M. E. *Chem. Mater.* **1998**, *10*, 2235−2250.
(9) Weiss, D. S.; Cowdery, J. R.; Young, R. H. In *Electron Transfer in Chemistry*; Balzani, V., Ed.; Wiley-VCH: Weinheim, 2001; Vol. 5; pp 379−471.
(10) Thelakkat, M. *Macromol. Mater. Eng.* **2002**, *287*, 442−461.
(11) Lambert, C.; Nöll, G. *Synth. Met.* **2003**, *139*, 57−62.
(12) Lambert, C.; Nöll, G.; Hampel, F. *J. Phys. Chem. A* **2001**, *105*, 7751−7758.
(13) Lambert, C.; Nöll, G.; Kriegisch, V.; Zabel, M.; Hampel, F.; Schmälzlin, E.; Bräuchle, C.; Meerholz, K. *Chem. Eur. J.* **2003**, *9*, 4232−4239.
(14) Bonvoisin, J.; Launay, J.-P.; Verbouwe, W.; Van der Auweraer, M.; De Schryver, F. C. *J. Phys. Chem.* **1996**, *100*, 17079−17082.
(15) Bonvoisin, J.; Launay, J.-P.; Van der Auweraer, M.; De Schryver, F. C. *J. Phys. Chem.* **1994**, *98*, 5052−5057, see also correction **1996**, *100*, 18006.
(16) Blackstock, S. C.; Selby, T. D. In *Magnetic Properties of Organic Materials*; Lahti, P. M., Ed.; Marcel Dekker: New York, 1999; pp 165−178.
(17) Stickley, K. R.; Blackstock, S. C. *Tetrahedron Lett.* **1995**, *36*, 1585−1588.
(18) Stickley, K. R.; Blackstock, S. C. *J. Am. Chem. Soc.* **1994**, *116*, 11576−11577.
(19) Selby, T. D.; Blackstock, S. C. *Org. Lett.* **1999**, *1*, 2053−2055.
(20) Wienk, M. M.; Janssen, R. A. *J. Am. Chem. Soc.* **1997**, *119*, 4492−4501.
(21) Bushby, R.-J. In *Magnetism: Molecules to Materials II*; Miller, J. S., Drillon, M., Eds.; Wiley-VCH: Weinheim, Germany, 2001; pp 149−187.
(22) Selby, T. D.; Blackstock, S. C. *J. Am. Chem. Soc.* **1999**, *121*, 7152−7153.
(23) Selby, T. D.; Stickley, K. R.; Blackstock, S. C. *Optics Lett.* **2000**, *2*, 171−174.
(24) Ito, A.; Urabe, M.; Tanaka, K. *Angew. Chem.* **2003**, *115*, 951−954.
(25) Hauck, S. I.; Lakshmi, K. V.; Hartwig, J. F. *Org. Lett.* **1999**, *1*, 2057−2060.
(26) Michinobu, T.; Takahashi, M.; Tsuchida, E.; Nishide, H. *Chem. Mater.* **1999**, *11*, 1969−1971.
(27) Selby, T. D.; Kim, K.-Y.; Blackstock, S. C. *Chem. Mater.* **2002**, *14*, 1685−1690.
(28) Kim, K.-Y.; Hassenzahl, J. D.; Selby, T. D.; Szulczewski, G. J.; Blackstock, S. C. *Chem. Mater.* **2002**, *14*, 1691−1694.
(29) Plater, M. J.; Jackson, T. *Tetrahedron* **2003**, *59*, 4687−4692.
(30) Ohsawa, Y.; Ishikawa, M.; Miyamoto, T.; Murofushi, Y.; Kawai, M. *Synth. Met.* **1987**, *18*, 371−374.
(31) Louie, J.; Hartwig, J. F.; Fry, A. J. *J. Am. Chem. Soc.* **1997**, *119*, 11695−11696.
(32) Katsuma, K.; Shirota, Y. *Adv. Mater.* **1998**, *10*, 223−226.
(33) Wu, I.-Y.; Lin, J. T.; Tao, Y.-T.; Balasubramaniam, E. *Adv. Mater.* **2000**, *12*, 668−669.
(34) Chen, C. H.; Shi, J.; Tang, C. W. *Macromol. Symp.* **1997**, *125*, 1−48.
(35) Selby, T. D.; Blackstock, S. C. *J. Am. Chem. Soc.* **1998**, *120*, 12155−12156.
(36) Krys, B.; S, T. *J. Org. Chem.* **2003**, *68*, 5559−67.

10.1021/ja0511570 CCC: $30.25

Chart 1

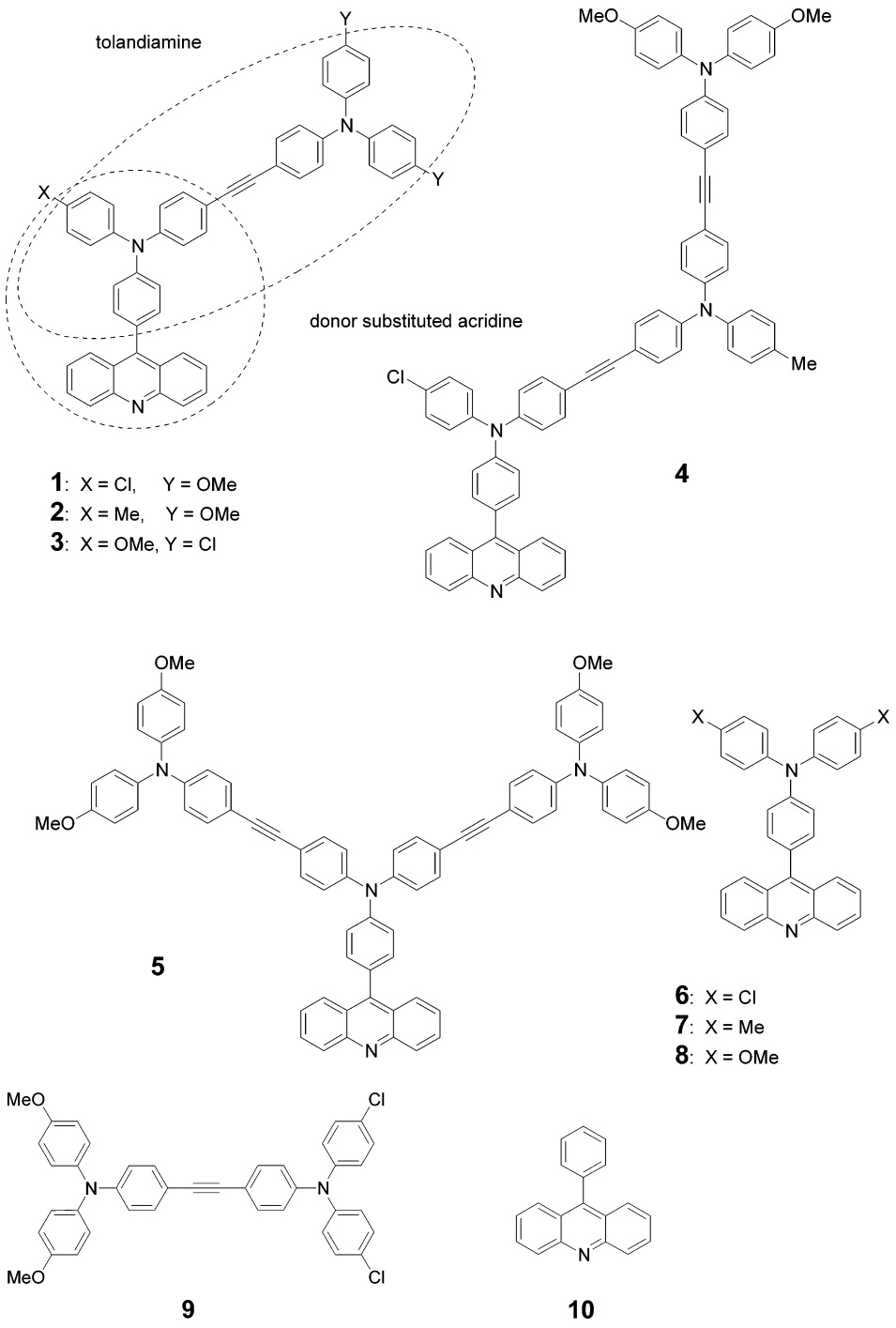

because triarylamines possess relatively low internal reorganization energy.[37,38] Therefore, HT processes are expected to be rather quick which will favor photoinduced charge separation processes over other competing processes. On the other hand, if the back electron transfer is in the Marcus inverted region, a small reorganization energy will slow the back electron transfer and will lead to long-lived charge separated states. Our investigations illustrate a first step how to construct an artificial light-driven system based on triarylamines that might be able to induce the long-range separation of opposite charges upon irradiation. So far, most systems that aim to mimic basic aspects of natural photosynthetic reaction centers use porphyrine chromophores in close analogy to their natural examples.[39] Only a few systems are known that incorporate triarylamine units.[40−48]

(37) Eberson, L. *Electron-Transfer Reactions in Organic Chemistry*; Springer: Berlin (Germany), 1987.
(38) Lin, B. C.; Cheng, C. P.; Lao, Z. P. M. *J. Phys. Chem. A* **2003**, *107*, 5241−5251.
(39) Gust, D.; Moore, T. A.; Moore, A. L. In *Electron Transfer in Chemistry*; Balzani, V., Ed.; Wiley-VCH: Weinheim (Germany), 2001; Vol. 3; p 272.
(40) Ramos, A. M.; Meskers, S. C. J.; van Hal, P. A.; Knol, J.; Hummelen, J. C.; Janssen, R. A. J. *J. Phys. Chem. A* **2003**, *107*, 9269−9283.
(41) Ramos, A. M.; Beckers, E. H. A.; Offermans, T.; Meskers, S. C. J.; Janssen, R. A. J. *J. Phys. Chem. A* **2004**, *108*, 8201−8211.
(42) Ohno, T.; Moriwaki, K.; Miyata, T. *J. Org. Chem.* **2001**, *66*, 3397−3401.
(43) Lor, M. V.; Lucien; Pilot, R.; Fron, E.; Jordens, S.; Schweitzer, G.; Weil, T.; Müllen, K.; Verhoeven, J. W.; Van der Auweraer, M. V.; De Schryver, F. C. *J. Phys. Chem. B* **2004**, *108*, 10721−10731.

In this study, we refrain from employing subunits that resemble the well-known natural systems and turn to completely artificial chromophores and redox centers which are more likely to be incorporated in future optoelectronic devices that shall build up an electrical potential upon irradiation.

The cascade structures **1**−**5** which we have designed are drawn in Chart 1 together with some reference systems. The principal features of the cascade systems are the fluorescent donor substituted acridine chromophore and the triarylamine cascade. The triarylamine units are connected by triple bonds in order to ensure an essentially rigid structure of the whole cascade with fixed HT distances. To illustrate our conceptual approach we divide the chromophores into the following subunits: acridine acceptor (**A**), the first triarylamine attached to the acridine (**Tara1**), the second, and third triarylamine (**Tara2** and **Tara3**) which are farther apart; two triarylamine groups connected by a triple bond yield a tolandiamine (e.g., **Tara1**-≡-**Tara2**). While the HT distances are fixed in **1**−**3** and **5** by the almost rigid structure it is not in **4** in which the N(acridine)···N(Tara3) distance can vary between ca. 23 and 29 Å, depending on the conformer.

The donor substituted acridine fluorophore (**A-Tara1**) is a strong oxidizing agent in the first excited charge transfer (CT) singlet state. This locally excited singlet state is expected to oxidize the adjacent triarylamine moiety (**Tara2**) which is attached to the donor substituted acridine by an acetylene spacer. We use donor substituted acridine dyes because their photophysics are reasonably well understood thanks to the work of Herbich and Kapturkiewicz[49] (hereafter called HK). These authors investigated a series of dialkylamino substituted phenylacridines by fluorescence spectroscopy. The local redox potential of the triarylamine units is tuned by substituents (Cl, Me, MeO) in para position of the phenyl rings so as to form two short (**1**, **2**) and one long (**4**) cascade with downhill hole transport gradient, that is, the triarylamine moiety which is farthest apart from the acridine has the lowest redox potential, i.e., it is more easily oxidized than the triarylamines adjacent to the acridine. In a recent study, we showed that the redox potentials of triarylamine in tolandiamines may span a range of 400 mV depending on the substituents.[50] For comparison, we also synthesized a branched dendrimeric system (**5**) as well as a short cascade with uphill redox gradient (**3**). The photophysical properties of these cascades will be compared with **A-Tara1** subunits (**6**−**8**) as well as with tolandiamine (**9**) and phenylacridine (**10**).

Results and Discussion

A. Stationary Optical Properties. The absorption spectra of the **A-Tara1** species **6**−**8** show a moderately strong CT band around 25 000 cm^{-1} which can be ascribed to a charge transfer from the triarylamine donor to the acridine acceptor (see Figure 1 and Table 1).[49]

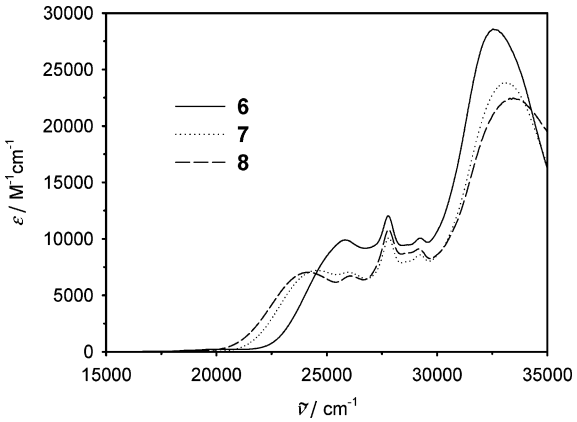

Figure 1. Absorption spectra of **6**−**8** in CH_2Cl_2.

Table 1. Absorption Maxima of **6**−**8**

	$\tilde{\nu}_{abs}/cm^{-1}$ ($\epsilon/M^{-1}cm^{-1}$)	$\tilde{\nu}_{abs}/cm^{-1}$ ($\epsilon/M^{-1}cm^{-1}$)	$\tilde{\nu}_{abs}/cm^{-1}$ ($\epsilon/M^{-1}cm^{-1}$)
	6	**7**	**8**
C_6H_{12}	26200 (10400)	25100 (9050)	24700 (6700)
Bu_2O	26100 (10300)	25100 (8490)	24600 (6830)
MTBE	26200 (10600)	25300 (8640)	24600 (7270)
1,4-dioxane	25900 (9980)	24900 (8030)	24400 (7410)
Et_2O	26100 (10700)	25300 (8210)	24700 (7580)
EtOAc	26000 (10200)	25200 (8100)	24600 (7630)
THF	26000 (9950)	24900 (7810)	24300 (7070)
CH_2Cl_2	25800 (9780)	24600 (7160)	24100 (6940)
DMF	25900 (8980)	24700 (7710)	24200 (6880)
DMSO	25700 (8560)	24400 (6550)	

The sharp peaks at ca. 26 000, 28 000, and 29 000 cm^{-1} stem from localized excitations of phenylacridine (**10**) and the broad and very intense peak at ca. 33 000 cm^{-1} is due to a localized triarylamine excitation. The CT bands are somewhat stronger red shifted with MeO substituents than with Me or Cl, that is, the donor strength of the triarylamine unit can be tuned by the para substituents attached to the phenyl rings.

The CT bands of **6**−**8** are moderately positive solvatochromic (e.g., **6**: 26 200 cm^{-1} in C_6H_{12} and 25 700 cm^{-1} in DMSO) which indicates an increase in dipole moment upon excitation. Fluorescence spectra of all compounds were measured at the excitation energy of the CT band maximum. Much in contrast to 9-phenylacridine **10** which is practically nonfluorescent, the donor substituted compounds **6**−**8** show strong fluorescence with high quantum yields (see Table 2). The fluorescence spectra of **6**−**8** are strongly positive solvatochromic and display a large Stokes shift (see e.g., Figure 2 for the fluorescence spectra of **6**, the full data set for all compounds is given in Table 2) which is stronger for **8** and **7** than for **6**. This Stokes shift indicates a major reorganization in the excited state. HK[49] explain this behavior by a solvent dependent mixing of a locally excited state and a CT state with a different degree of planarization in the excited state while the ground state is generally nonplanar. Here, we simply state that AM1 computations yield two ground-state minima for **8** that are very close in energy but differ in their relative orientation of the dianisylamino group to the acridine moiety, coplanar vs perpendicular, the latter being in accordance with the X-ray crystal structure investigation (see Supporting Information). If cyclohexane is excluded, then a plot of the fluorescence energy vs the solvent parameters according to Lippert and Mataga (eq 1)[51] yields a reasonable linear correlation (Figure 3 and Table 3). Cyclohexane is excluded as

(44) Sandanayaka, A. S. D.; Sasabe, H.; Araki, Y.; Furusho, Y.; Ito, O.; Takata, T. *J. Phys. Chem. A* **2001**, *108*, 5145−5155.
(45) Luo, H.; Fujitsuka, M.; Araki, Y.; Ito, O.; Padmawar, P.; Chiang, L. Y. *J. Phys. Chem. B* **2003**, *107*, 9312−9318.
(46) Komamine, S.; Fujitsuka, M.; Ito, O. M.; Miyata, K.; Toshiyuki; Ohno, T. *J. Phys. Chem. A* **2000**, *104*, 11497−11504.
(47) Lor, M.; Thielemans, J.; Viaene, L.; Cotlet, M.; Hofkens, J.; Weil, T.; Hampel, C.; Müllen, K.; Verhoeven, J. W.; Van der Auweraer, M.; De Schryver, F. C. *J. Am. Chem. Soc.* **2002**, *124*, 9918−9925.
(48) Sandanayaka, A. S. D.; Matsukawa, K.; Ishii, T.; Mataka, S.; Araki, Y.; Ito, O. *J. Phys. Chem. B* **2004**, *108*, 19995−20004.
(49) Herbich, J.; Kapturkiewicz, A. *J. Am. Chem. Soc.* **1998**, *120*, 1014−1029.
(50) Lambert, C.; Nöll, G. *J. Chem. Soc., Perkin Trans. 2* **2002**, 2039−2043.

Table 2. Steady State and Time Resolved Optical Properties of **1**−**8**

	$\tilde{\nu}_f$/cm^{-1}	Φ_f	τ_f/ns	k_f/10^8 s^{-1}	k_{nr}/10^8 s^{-1}	$\tilde{\nu}_f$/cm^{-1}	Φ_f	τ_f/ns	k_f/10^8 s^{-1}	k_{nr}/10^8 s^{-1}
			1					**2**		
C_6H_{12}	22400	0.23	1.5	1.5	5.1	21900	0.42	1.7	2.5	3.4
Bu_2O	20500	0.38				20000	0.53			
MTBE	19400	0.37	5.9	0.63	1.1	19100	0.49	4.8	1.0	1.0
1,4-dioxane	19500	0.49	5.4	0.91	0.94	18900	0.67	6.4	1.0	0.52
Et_2O	18100	0.10				17800	0.22			
EtOAc	17800	0.08	4.7	0.16	2.0	17500	0.27			
THF	17300	0.06	5.0	0.12	1.9	17300	0.22	5.9	0.37	1.3
CH_2Cl_2	15700	0.01	0.8	0.13	12	15500	0.02	0.7	0.28	14
PrCN										
DMF										
DMSO										
			3					**4**		
C_6H_{12}	22000	0.42	1.8	2.4	3.2	22600	0.18	1.0	1.8	8.2
Bu_2O	20000	0.51				21000	0.30			
MTBE	19000	0.67	4.9	1.4	0.68	20000	0.32	4.3	0.75	1.6
1,4-dioxane	18900	0.58	6.3	0.92	0.67	19800	0.42	4.7	0.90	1.2
Et_2O	17800	0.50	6.9	0.73	0.72	18900	0.20			
EtOAc	17300	0.36				18400	0.22	8.0	0.27	0.98
THF	17200	0.46	7.2	0.63	0.76	18300	0.13	9.2	0.14	0.95
CH_2Cl_2	15700	0.18	7.4	0.25	1.1	16000	0.02	4.8	0.032	2.1
PrCN										
DMF	14800	0.01								
DMSO										
			5					**6**		
C_6H_{12}	21800	0.40	1.9	2.1	3.2	23000	0.14	0.55	2.6	16
Bu_2O	20300	0.74	3.4	2.2	0.77	21800	0.26			
MTBE	19100	0.31	4.5	0.69	1.5	20900	0.38	1.9	2.0	3.3
1,4-dioxane	19000	0.47	6.0	0.78	0.88	20600	0.52	3.2	1.6	1.5
Et_2O	17900	0.23				20100	0.47			
EtOAc	17700	0.18	6.3	0.29	1.3	19100	0.86	6.0	1.2	0.43
THF	17400	0.15	6.9	0.22	1.2	19200	0.74	5.7	1.5	0.24
CH_2Cl_2	15300	0.01	1.0	0.10	9.9	18200	0.90	9.3	0.97	0.10
PrCN						17100	0.74			
DMF						16500	0.72	11.4	0.63	0.25
DMSO						15900	0.65	11.6	0.56	0.30
			7					**8**		
C_6H_{12}	22100	0.28	1.3	2.2	5.5	21300	0.34	2.0	1.7	3.3
Bu_2O	20400	0.41				18900	0.56			
MTBE	19400	0.56	4.9	1.1	0.90	17800	0.66	6.7	0.99	0.51
1,4-dioxane	19000	0.72				17600	0.71			
Et_2O	18300	0.63				16600	0.34			
EtOAc	17700	0.67				16100	0.20			
THF	17700	0.76	8.9	0.86	0.27	16000	0.29	6.2	0.47	1.1
CH_2Cl_2	16100	0.58	12.4	0.46	0.34	14800	0.05	2.4	0.21	4.0
PrCN	15600	0.28								
DMF	15000	0.10								
DMSO	14800	0.07	2.8	0.23	3.3					

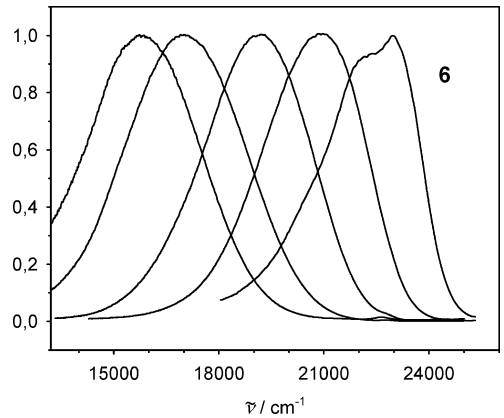

Figure 2. Normalized fluorescence spectra (solid lines) of **6** from left to right in DMSO, PrCN, THF, MTBE, C_6H_{12}.

it gives values which are significantly too low; this effect might have to do with changes in solute geometry in this very apolar solvent. In eq 1 $\tilde{\nu}_f$ is the fluorescence energy maximum, $\tilde{\nu}_f^{vac}$ is the fluorescence energy maximum in vacuum, μ_g and μ_e are the ground state and excited-state dipole moments, respectively, which are assumed to be parallel, a_0 is the effective radius of the solute, n is the refractive index and ϵ is the permittivity of the solvent. The slopes of the Lippert−Mataga correlations for **6**−**8** are quite similar (see Figure 3 and Table 3). An effective solute radius of 7 Å (estimated from an AM1 computation) yields a dipole moment of 31 D for the excited state. The ground state has a dipole moment of 4−5 D depending on the conformation (see above) estimated by AM1 computations. Thus, the dipole moment difference of ca. 26 D roughly corresponds to the transfer of a unit charge from the triarylamine nitrogen to the acridine center. Therefore, we can best describe the CT state by **(A)**$^-$**-(Tara1)**$^+$. In general, the stationary

(51) Suppan, P.; Ghoneim, N. *Solvatochromism*; The Royal Society of Chemistry: Cambridge, 1997.

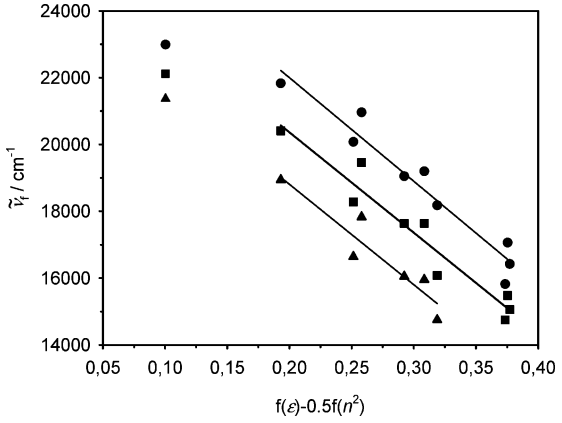

Figure 3. Lippert−Mataga plot for **6** (circles), **7** (squares), and **8** (triangles). The solvents are from left to right: C_6H_{12}, Bu_2O, Et_2O, MTBE, EtOAc, THF, CH_2Cl_2, DMSO, PrCN, DMF. Cyclohexane is excluded from the correlation.

Table 3. Fitted Parameters from Eq 1

	$\tilde{\nu}_f^{vac}$/cm^{-1}	$(2\vec{\mu}_e(\vec{\mu}_e - \vec{\mu}_g))/4\pi\epsilon_0 hc a_0^3$/cm^{-1}
1	27120	−33330
2	26120	−30470
3	25840	−29570
4	27620	−32710
5	26730	−32520
6	28200	−31020
7	26380	−30060
8	24820	−30050

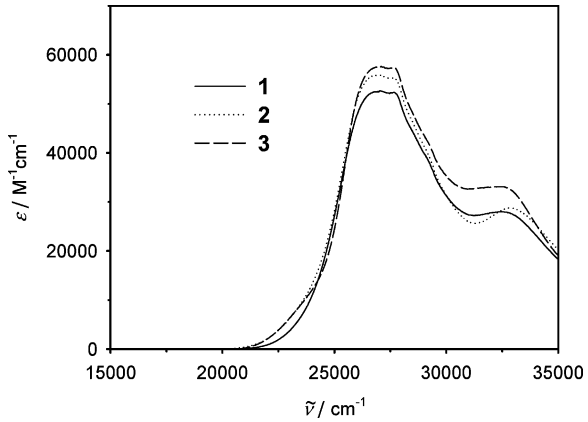

Figure 4. Absorption spectra of **1**−**3** in CH_2Cl_2.

absorption and fluorescence behavior of **6**−**8** is analogous to the dialkylamino substituted species described by HK.[49]

$$\tilde{\nu}_f = \tilde{\nu}_f^{vac} - \frac{2\mu_e(\mu_e - \mu_g)}{4\pi\epsilon_0 hc a_0^3}\left(f(\epsilon) - \frac{1}{2}f(n^2)\right) \text{ with}$$

$$f(\epsilon) = \frac{\epsilon - 1}{2\epsilon + 1} \text{ and } f(n^2) = \frac{n^2 - 1}{2n^2 + 1} \quad (1)$$

The absorption spectra of the cascades **1**−**5** (see Figures 4 and 5) are much less structured than those of **6**−**8** due to severe band overlap. The main feature that is added is a very intense band at ca. 27 000 cm^{-1} which is due to the tolandiamine moiety. This band overlaps strongly with the CT band at ca. 25 000 cm^{-1} which is only seen as a low-energy tail of the tolandiamine band which prevents a reasonable band deconvolution. From Figure 4, it is obvious that the substitution pattern has only a marginal influence on the absorption spectra with exception of the low-energy tail which is more intense in **3** due to the MeO substituent at **Tara1** which makes it a stronger donor compared to **Tara1** in **1** and **2**. The absorption spectra of **4** and **5** are quite similar because both species have the same number of **Tara** groups and tolandiamine units. This observation supports the conceptual approach of dividing the cascades into the above-mentioned moderately interacting units.

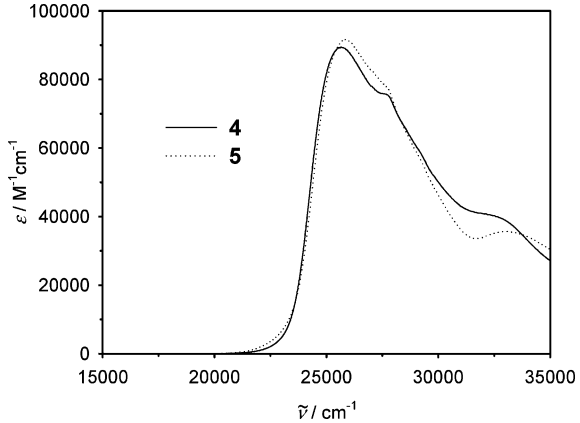

Figure 5. Absorption spectra of **4** and **5** in CH_2Cl_2.

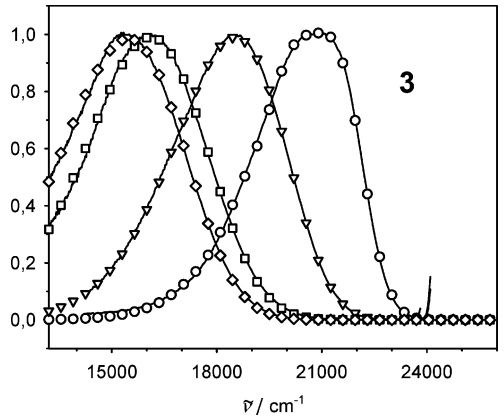

Figure 6. Reduced $(I(\tilde{\nu}_f)/\tilde{\nu}_f^3$ vs $\tilde{\nu}_f)$ and normalized fluorescence spectra (solid lines) of **3** from left to right in THF, Et_2O, Bu_2O, C_6H_{12}, and simulation by eq 2 (symbols).

The fluorescence spectra of **1**−**5** (see Figure 6) are strongly solvatochromic and are very similar in energy and band shape to those of **6**−**8**, irrespective of the excitation energy. However, while there are significant differences in the Stokes shift of **6**−**8** due to strong substituent effects, the fluorescence energy maxima for **1**−**5** are very similar in a given solvent. The slopes of the Lippert−Mataga plots of **1**−**5** are also in good agreement with those of **6**−**8**. Excitation spectra of all compounds are identical to the absorption spectra and prove complete energy transfer to the S_1 state, irrespective of excitation energy. In addition, no fluorescence from other states, e.g., local tolandiamine states was observed which should occur between 25 000 and 20 000 cm^{-1}. For comparison, the fluorescence of tolandiamine **9** occurs between 24 700 cm^{-1} (cyclohexane) and 20 000 cm^{-1} (DMSO) with quantum yields of 0.60 and 0.70. Altogether, these features prove that the fluorescent state in the cascades has the same electronic nature as that in the **A-Tara1** species **6**−**8**, i.e., all cascades emit from a more or less dipolar CT state localized in the **A-Tara1** moiety.

Table 4. Reorganization Energies and Free Energy Difference of **3** as Derived from Eq 2

	λ_v/cm^{-1}	λ_s/cm^{-1}	ΔG_{00}/cm^{-1}	$\tilde{\nu}_v$/cm^{-1}
C_6H_{12}	1100	1240	−23250	1450
Bu_2O	1240	2080	−22510	1400
MTBE	1210	2620	−21980	1400
1,4-dioxane	1100	2600	−21740	1400
Et_2O	1140	3670	−21790	1400
EtOAc	1170	3740	−21340	1400
THF	1090	3650	−21080	1400
CH_2Cl_2[a]	1440	3400	−19520	1400

[a] Bad signal-to-noise ratio.

To extract the reorganization energy λ_s associated with any low-frequency vibrations (such as solvent and low energy solute motions) and the reorganization energy λ_v associated with any high energy vibrations (bond length and angle distortions) as well as the free energy difference ΔG_{00} between the relaxed excited CT and the ground-state we applied the vibrational coupling theory[52−54] based on a Golden rule expression where μ_{fl} is the fluorescence transition moment and S is the Huang−Rhys factor $\lambda_v/\tilde{\nu}_v$.The fluorescence spectra were fitted by eq 2, where $\tilde{\nu}_v$ is an averaged high-frequency mode associated with λ_v.

$$I_{fl}/\tilde{\nu}^3 = \frac{16 \times 10^6 \pi^3}{3\epsilon_0} \frac{n(n^2+2)^2}{9} \mu_{fl}^2 \sum_{j=0}^{\infty} \frac{e^{-S} S^j}{j!} \sqrt{\frac{1}{4\pi hc\lambda_s kT}} \exp\left[- \frac{hc(j\tilde{\nu}_v + \lambda_s + \tilde{\nu} + \Delta G_{00})^2}{4\lambda_s kT} \right] \quad (2)$$

The fitted reorganizational parameters are collected in Table 4 for **3** and the fits are displayed in Figure 6. An averaged vibration $\tilde{\nu}_v$ = ca. 1400 cm^{-1} was used for the fits which roughly correlates to a C−N vibration. Although the partitioning of the total reorganization energy into λ_s and λ_v is somewhat arbitrary, the free energy ΔG_{00} is rather accurate and decreases with increasing solvent polarity. However, the sum of both reorganization energies compares well with those of tetraaryltolandiamine radical cations in CH_2Cl_2 which is ca. 6000 cm^{-1}.[50] Similar observations are true for all other derivatives **1**, **2**, and **4**−**8**.

B. Redox Properties. To gain insight into the energy of localized states with radical cation or radical anion character we measured the redox potentials of **1**−**8** by cyclic voltammetry (CV) in CH_2Cl_2/0.2 M TBAH solution vs Fc/Fc$^+$. The corresponding redox potentials are collected in Table 5 where they are grouped according to their redox potential range. An interpretation as to which triarylamine moiety the given potentials refer is also given in parentheses. The relatively narrow range in which the redox potential for a given type of triarylamine groups occurs shows that the coupling between the triarylamine groups is relatively small compared to the influence of the substituents (Cl, Me, MeO). The redox processes at ca. −2200 mV refer to chemically irreversible reductions of the acridine acceptor, those above 1000 mV refer to the second oxidation of the triarylamine that is most easily oxidized.

(52) Jortner, J.; Bixon, M. *J. Chem. Phys.* **1988**, *88*, 167−170.
(53) Gould, I. R.; Noukakis, D.; Gomez-Jahn, L.; Young, R. H.; Goodman, J. L.; Farid, S. *Chem. Phys.* **1993**, *176*, 439−456.
(54) Marcus, R. A. *J. Phys. Chem.* **1989**, *93*, 3078−3086.

Table 5. Redox Potentials of **1**−**8** in CH_2Cl_2/0.2 M TBAH vs Fc/Fc$^+$, v = 250 mV s^{-1}[a]

	$E_{1/2}^{red}$/mV	$E_{1/2}^{ox,1}$/mV	$E_{1/2}^{ox,2}$/mV	$E_{1/2}^{ox,3}$/mV	$E_{1/2}^{ox,4}$/mV
1	−2160[b]	260 (**Tara2**)		640 (**Tara1**)	1120[b]
2	−2130[b]	250 (**Tara2**)	530 (**Tara1**)		1100[b]
3	−2150[b]	400 (**Tara1**)		620 (**Tara2**)	
4	−2160[b]	240 (**Tara3**)	480 (**Tara2**)	680 (**Tara1**)	1030[b]
5	−2160[b]	270[c] (**Tara2**)		630 (**Tara1**)	1050[b]
6	−1730[b]			690 (**Tara1**)	1320[b]
7	−2080[b]		460 (**Tara1**)		
8	−2140[b]	290 (**Tara1**)			1020[b]

[a] The assignments in parentheses refer to the triarylamine group that is oxidized at the given potential. [b] Irreversible process, peak potential. [c] Two electron transfer, not resolved.

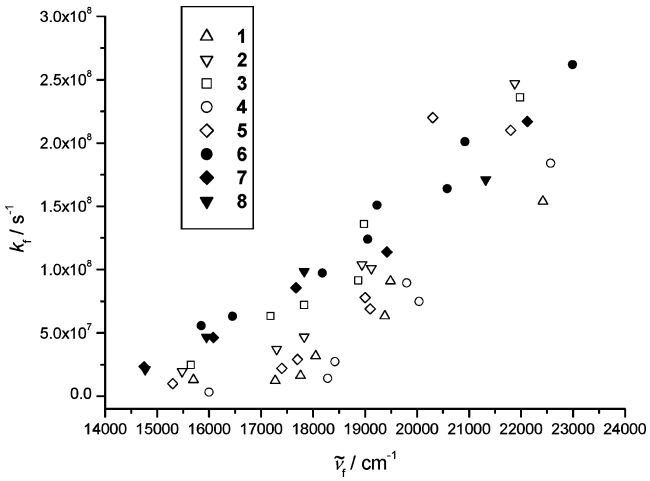

Figure 7. Rate constant of the radiative process k_f vs fluorescence transition energy $\tilde{\nu}_f$ for **1**−**8** in different solvents.

The redox potentials for **1**, **2**, **4**, and **5** show that the energy cascade for an excited state with predominantly localized triarylamine radical cation character is downhill for the migration of a hole from **Tara1** to **Tara2** and **Tara3**. Much in contrast it is uphill for **3** where the triarylamine substituents (Cl, MeO) are exchanged in comparison with **1**.

C. Time-Resolved Fluorescence Properties. Time-resolved fluorescence decays τ_f for **1**−**8** were measured in the nanosecond regime in selected solvents that cover the range from totally apolar (cyclohexane) to highly polar (DMSO). In all cases a single-exponential decay was observed. In addition, we measured the fluorescence quantum yield Φ_f in all solvents. The quantum yields vary depending on the solvent from being low in apolar solvents and in rather polar solvents with a maximum of quantum yield in between up to 0.90 (see Table 2). From both quantities, τ_f and Φ_f we calculated the rate constant for the radiative (k_f) and nonradiative decay (k_{nr}) according to eqs 3 and 4.

$$\Phi_f = \frac{k_f}{k_f + k_{nr}} \quad (3)$$

$$\tau_f = \frac{1}{k_f + k_{nr}} \quad (4)$$

Both a plot of k_{nr} and of k_f for compounds **1**−**8** in different solvents vs the fluorescence energy shows a relatively narrow scattering range of data points (see Figures 7 and 8), Therefore, it is obvious that the photophysics of **1**−**8** in the nanosecond

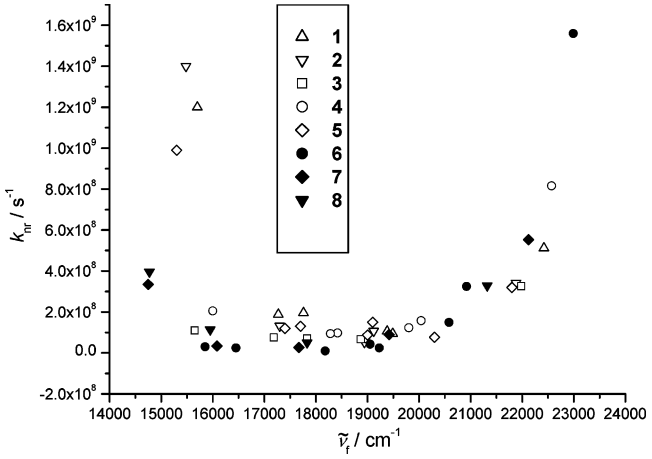

Figure 8. Rate constant of the nonradiative process k_{nr} vs fluorescence transition energy $\tilde{\nu}_f$ for **1**−**8** in different solvents.

time domain are energy controlled, that is, the energy of the fluorescent **A-Tara1** located CT state dominates its deactivation kinetics. The fluorescence energy can either be tuned by substituents (Cl, Me, MeO, Tara2, etc.) or by the solvent (apolar > polar).

As one can see in Figure 8 k_{nr} is practically constant between 16 000 and 20 000 cm^{-1} while above 20 000 cm^{-1} k_{nr} rises strongly. This increase with increasing fluorescence energy was also found by HK in carbazole derivatives[55] and was interpreted by a dominating intersystem crossing (ISC) from the fluorescent CT state to a lower lying triplet state. However, as we will see below we did not find any evidence in the transient absorption (TA) spectra for the population of a long-lived triplet state. The reason of the k_{nr} increase for $\tilde{\nu}_f$ > 20 000 cm^{-1} thus remains cumbersome. For the energies below 16 000 cm^{-1} the set of derivatives **1**−**8** splits into two groups: those derivatives whose nonradiative rate constant remains essentially constant or increases slightly (**6**−**8** and **3**) and those of which k_{nr} dramatically increases by roughly one order of magnitude (**1**,**2**,**5**). Obviously, the above-mentioned energy control of deactivation kinetics fails for the latter group of compounds. For compound **4** there is no data point low enough in energy in order to decide to which group it belongs, however, we will present evidence below that **4** also is likely to belong to the latter group.

The increase in k_{nr} for **1**, **2**, **4**, and **5** is due to an additional deactivation pathway. Though superficially very similar, the contrasting k_{nr} behavior of **3** vs **1** and **2** shows that the lack of an additional deactivation pathway in **3** is due to the fact that **3** displays an uphill gradient for hole migration while **1** and **2** possess a downhill gradient. Therefore, we assume that the additional nonradiative deactivation pathway is a hole transfer (HT) from **Tara1** to **Tara2** in **1** and **2**. This hole migration is only downhill in rather polar solvents, because, in contrast to the oxidation processes observed in CV, hole migration from an excited **A-Tara1** CT state involves a charge separation which is unfavorable in apolar solvents. Much in contrast, the hole migration is uphill for **3** in all solvents and, thus, no additional nonradiative deactivation is observed. To assess whether a photoexcitation process followed by a hole migration can be responsible for the above-mentioned additional fluorescence quenching effect we employ the Rehm−Weller equation. Equation 5 can be used to estimate the free energy for the PET-hole migration process $\Delta G°$ by subtracting the redox potential difference ΔE of donor (**Tara2**) and acceptor (**A**) from the free energy difference of the ground and excited CT state potential energy surface minima ΔG_{00}.[56] The redox potential difference can be obtained from the values in Table 5 which refer to CH_2Cl_2/0.2 TBAH solution: ΔE = 0.260 V (**Tara2**) − (−2.160 V (**A**)) = 2.420 V for **1** and ΔE = 0.620 V (**Tara2**) − (−2.150 V (**A**)) = 2.770 V for **3**. The free energy ΔG_{00} in CH_2Cl_2 is taken from the fits of eq 2 (Table 4) which can be estimated to be ca. 20 000 cm^{-1} for **1** (the ΔG_{00} value for CH_2Cl_2 could not be determined for **1** because of the bad signal-to-noise ratio of the fluorescence spectrum in CH_2Cl_2) and 19 520 cm^{-1} for **3**.

Table 6. Hole Transfer Rate from **Tara1** to **Tara2** in **1**−**5** from Fluorescence Lifetime Measurements[a]

	$k_{HT} = k_{nr}(\mathbf{x}) - k_{nr}(\mathbf{y})/10^8\ s^{-1}$ *x*/*y*				
	1/6	**2/7**	**3/8**	**4/6**	**5/7**
C_6H_{12}	(−)	(−)	(−)	(−)	(−)
MTBE	(−)	0.1	0.17	(−)	0.6
1,4-dioxane	(−)			(−)	
EtOAc	1.6			0.55	
THF	1.7	1.0	(−)	0.71	0.93
CH_2Cl_2	12	14	(−)	2.0	9.6

[a] (−) indicates no hole transfer (k_{HT} is negative).

$$\Delta G° = 8065.5[E°(\mathbf{Tara2}) - E°(\mathbf{A})] - \Delta G_{00} \qquad (5)$$

Eq 5 yields $\Delta G°$ = −500 cm^{-1} for **1** but +2820 cm^{-1} for **3**. Although the Rehm−Weller equation only allows a very rough estimate of the free energy of a PET the exergonic value for **1** suggests that a hole migration from the **A-Tara1** CT state to **Tara2** is energetically favorable while the endergonic value for **3** explains why we cannot observe hole migration, and, consequently no additional fluorescence quenching pathway. The same holds true for **2** for which ΔG^0 = ca. −200 cm^{-1}. Because the cascade **4** and the dendrimer **5** possess very similar fluorescence energy properties and redox potential values we expect hole migration also to be possible in polar solvents. In fact, for **5** the rather high nonradiative rate constant suggests a similar process. For the cascade **4**, we were unable to measure the rate constant in a solvent more polar than CH_2Cl_2 for which the hole transfer is distinctly favorable. In any case, the free energy values derived by the Rehm−Weller equation for **1** and **2** are rather small so that small changes in the medium polarity can switch the system in a way that hole migration to **Tara1** or **Tara2** is favorable or unfavorable while for **3** it is an unfavorable uphill process independent of the solvent. From the fluorescence lifetime data (see Table 2) we can estimate the hole transfer rate k_{HT} from **Tara1** to **Tara2** in **1**−**5** by the difference between k_{nr} of these compounds and the reference compounds **6**−**8** as given in Table 6. The reference compounds were chosen as to match the **A-Tara1** moiety in **1**−**5** as close as possible. A negative sign of k_{HT} indicates that no hole migration is possible either because it is against the redox gradient as in **3** or it is because less polar solvents disfavor charge separation.

(55) Kapturkiewicz, A.; Herbich, J.; Karpiuk, J.; Nowacki, J. *J. Phys. Chem. A* **1997**, *101*, 2332−2344.

(56) Kavarnos, G. J. *Fundamentals of Photoinduced Electron Transfer*; VCH: Weilheim (Germany), 1993.

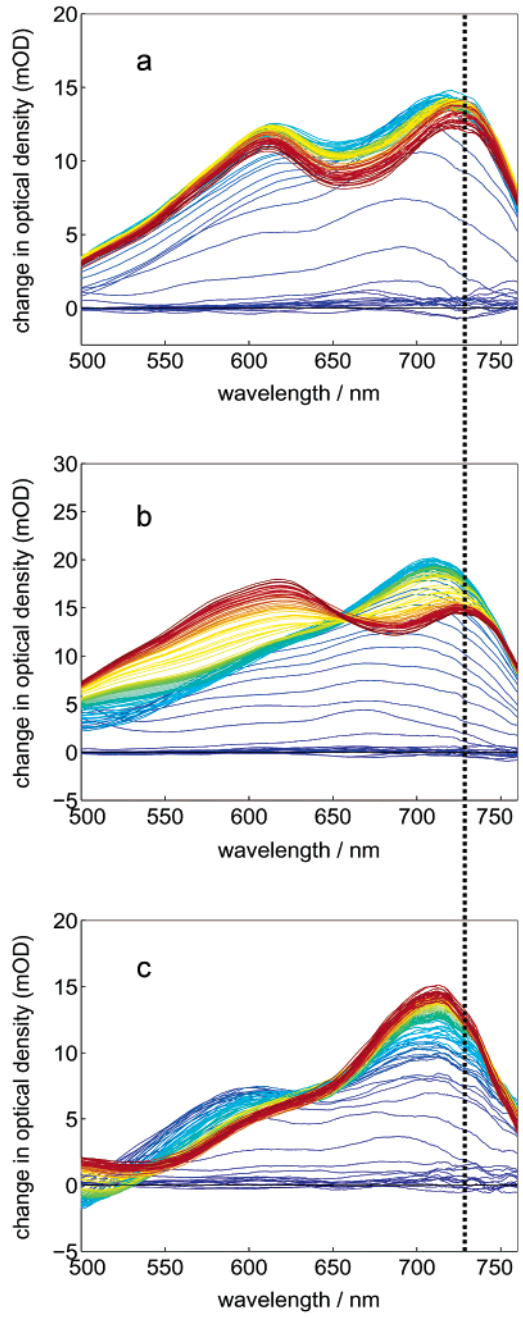

Figure 9. Temporal evolution of the pump−probe spectra of **8** in different solvents; (a) acetontrile, (b) benzonitrile, (c) MTBE, within the first 20 ps after excitation (step size: 60 fs). Early spectra are shown in blue/green and late spectra are shown in orange/red colors.

D. Femtosecond Pump−Probe Spectra. Excited-State Dynamics of 8. To elucidate the photophysical mechanisms in the model redox cascades it is crucial to investigate first the dynamics after photoexcitation in the acridine-triarylamine D−A systems without the tolandiamine "antenna". Figure 9 shows the temporal evolution of the pump−probe-spectra of **8** measured in three different solvents after excitation at 360 nm (27 800 cm^{-1}). Immediately after excitation there is a broad transient absorption band showing a weak bifurcation with weakly pronounced maxima centered around 610 and 690 nm. Note that this initial spectral distribution—which rises within the pulse duration of our experimental setup (∼80 fs)—is almost solvent independent (Figure 9a−c, blue spectra). After several 100 fs, however, the evolution becomes strongly solvent dependent. In acetonitrile (Figure 9a) the initial two peak distribution becomes more pronounced while the band at 690 nm undergoes a shift to 725 nm. Reference measurements on dianisylphenylamine have shown that the lowest excited singlet state of these compounds absorb at ∼700 nm. At the same time dianisylarylamine radical cations absorb at around 730 nm.[3] Hence, upon charge transfer in **8** one would expect to observe a dynamical shift in this spectral region. Acridine radical anions are known to have an absorption band at ∼610 nm.[57] Thus, the temporal evolution of **8** in acetonitrile reflects an ultrafast *photoinduced* (as opposed to *optical*) charge transfer from triarylamine to the acridine unit in less than 2 ps.

In benzonitrile (Figure 9b) the initial spectral bifurcation is merging into a pronounced band at 700 nm which reaches its maximum intensity after 500 fs. The onset of charge transfer is marked by a spectral shift of the amine radical cation band (accompanied by a drop in intensity) as well as by the rise of the band of the acridine radical anion (610 nm). In contrast to acetonitrile, where the charge-transfer process leads to a continuous spectral shift the results in benzonitrile reveal characteristic "two-level" kinetics with a well pronounced isosbestic point at 660 nm.

Finally, in MTBE we observe the rise of the triarylamine excited-state absorption band at 710 nm. However, the rise is not followed by a spectral shift toward 730 nm (triarylamine radical cation) and the acridine radical anion band around 610 remains absent as well. Consequently, there is no evidence for the population of a strongly dipolar CT state in MTBE.

From the results shown in Figure 9 the following mechanistic picture emerges. Excitation of **8** leads to a largely delocalized excited state with similar electronic (and geometrical) structure in acetonitrile, benzontrile and MTBE. Immediately after excitation, coupling to various nuclear modes (both internal and solvent modes) leads to energy localization on the time scale of 100 fs to 1 ps. The spectroscopic signatures found in the transient absorption spectra suggest that—in all three solvents—a locally excited (LE) triarylamine state is formed shortly after excitation. Reference measurements on dianisylphenylamine have shown that the lowest excited singlet state of these compounds absorb at ∼700 nm. In the polar acetonitrile, ultrafast energy localization competes with charge transfer which occurs on the same time scale. In benzonitrile, the thermodynamic driving force for CT is much smaller which leads to a reduced CT rate. Hence, energy localization and CT are clearly separable processes. Finally, in MTBE the thermodynamics for CT are highly unfavorable and thus the triarylamine excited-state cannot undergo efficient CT.

CT and Effect of Driving Force in Tolandiamine-Bridged Systems. Photoexcitation of **1**−**5** at the pump wavelength (360 nm = 27 800 cm^{-1}) initially populates a tolandiamine state (see Figure 10) because this unit has the highest absorptivity at this energy (see Figures 4 and 5). Hence, the tolandiamine units serve as antenna system. These tolandiamine states are expected to be the precursor states for ultrafast intramolecular energy transfer to the corresponding charge transfer states. Immediately after photoexcitation of **1** and **3** we observe a broad, structureless absorption between 500 and 700 nm (see Figure 10a). This band

(57) Shida, T. *Electronic Absorption Spectra of Radical Ions*; Elsevier: Amsterdam, 1988.

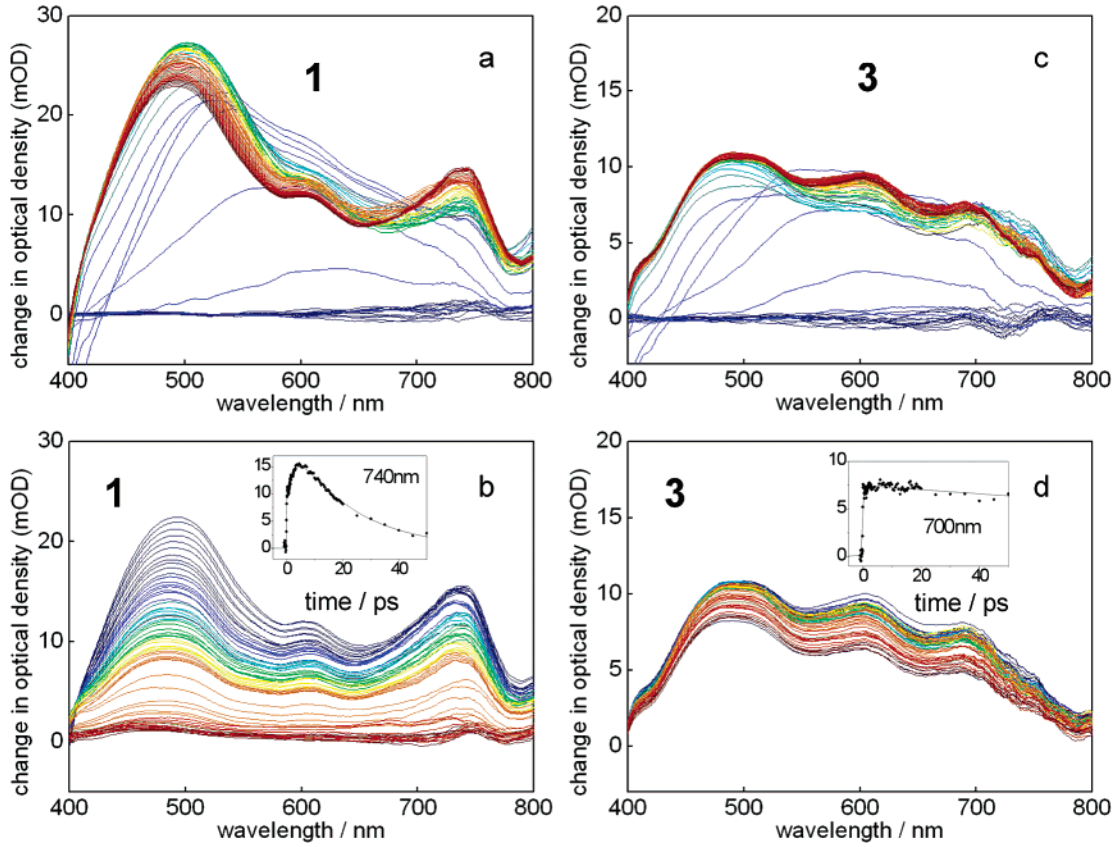

Figure 10. Temporal evolution of the pump−probe spectra of **1** (a, b) and **3** (c,d) in acetonitrile, the upper panels (a) and (c) show early spectra from −1.0 to 3 ps after excitation (60 fs step size). The lower panels (b) and (d) represent the spectra 3 to 130 ps after excitation (various step sizes). Early spectra in each panel are shown in blue/green and late spectra are shown in orange/red colors. The insets show the time-dependent absorption at 740 and 700 nm, respectively (see text for details).

represents the absorption of the unrelaxed Franck Condon state populations. After several 100 fs, there are three main transient absorption bands, the 610 nm (acridine radical anion), the 700−740 nm band (triarylamine radical cation), and a very intense band at 490 nm which must be assigned to excited-state absorption of the tolandiamine system. A similar transient absorption band at 480 nm is also visible in the spectra of tolandiamine **9** in MeCN. The fact that the tolandiamine band at 490 nm is present throughout the lifetime of the excited states of **1**−**5** must be viewed as a clear indication that the transient absorption spectra cannot be reconstructed by (diabatic) mixing of spectral reference components obtained from separate measurements. Hence, the electronic coupling between the chromophores is significant.

Figure 10 also displays the time-dependent transient absorption signal of the 740 nm band. In contrast to **8** (acetonitrile) where this band rises within the time resolution of our experimental setup the rise of this band in **1** is strongly biexponential, i.e., it shows a rise time of 4 ps (40%). This rise time must be interpreted as the hole transfer time from the triarylamine (**Tara1**) which is adjacent to the acridine to the terminal amine (**Tara2**).

Because of the substitution scheme in **3** hole transfer between the central and the terminal amine unit is thermodynamically unfavorable. Hence, a long-lived charge transfer state of the type $\mathbf{A}^{-}-(\mathbf{Tara1})^{+}-\mathbf{Tara2}$ is formed. Entirely consistent with this proposal is the fact, that the rise of the 700 nm band in **3** is not showing a ps component (see Figure 10 inset).

A comparison of the 740 and 700 nm transients of **1** and **3** (insets of Figure 10) reveals a significantly longer lifetime of the CT state of **3**. However, in addition to these differences the intensity ratio reveals also interesting information about the excited-state relaxation in **1** and **3**. Most obvious is the difference in the relevant contribution of the 610 nm band which is significantly stronger in **3** than in **1**, suggesting a more localized, twisted acridine radical anion in **3** than in **1**. In fact, this interpretation is in agreement with the rest of our data: In **3** the charge is only being transferred between the acridine and the adjacent **Tara1** amine unit. To establish a large dipole moment the acridine has to twist to electronically decouple from the rest of the aromatic system. This will result in a fairly pure acridine radical anion band. The CT state dipole moment of **1** is somewhat larger than that of **3** (see the larger slope of **1** vs **3** in the Lippert−Mataga plot, Table 3), however one has to bear in mind that the positive charge is delocalized much farther over the second amine unit. Hence, the negative charge on the acridine will also be delocalized. As a result, the radical anion character is "diluted" which is manifested in the reduced 610 nm band.

Effect of the Redox Cascade Extension. Figure 11 shows the temporal evolution of the pump−probe spectra of **4** and **5** in acetonitrile. The insets display the time-dependent transient absorption at 740 nm (triarylamine radical cation band). From a comparison of the symmetrical "doubly branched" system **5** with its single-branch analogue **1** it becomes clear that the spectral properties are very similar (both in time evolution and

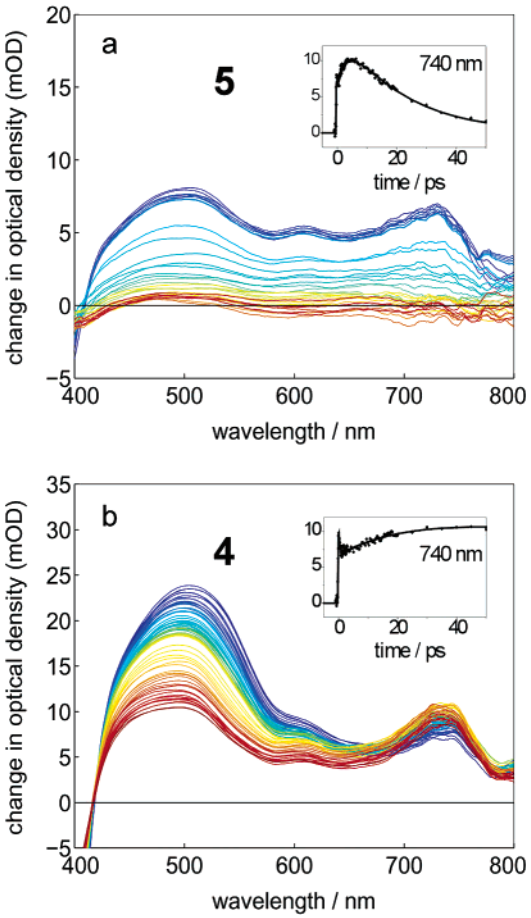

Figure 11. Temporal evolution of the pump−probe spectra of (a) **5** and (b) **4** in acetonitrile, 3 ps to 150 ps after excitation (various step sizes). Early spectra are shown in blue/green and late spectra are shown in orange/red colors. The insets show the time-dependent absorption at 740 nm (see text for details).

in spectral distribution) suggesting that the two tolandiamine branches are acting as independent substituents.

Figure 11b shows the pump−probe spectra of the extended redox system **4**. Most noticeable is the kinetic behavior (inset 11b) which differs qualitatively and quantitatively from all other systems. The instant rise of the 740 nm signal is followed by an ultrafast decay (200−300 fs) and then another slow rise with a time constant of 20 ps. These characteristics can be explained by assuming that the signal is a composite of two overlapping spectral contributions. Given the structure of **4** it seems reasonable to propose the following model: Photoexcitation at 360 nm of the tolandiamine units leads to two parallel processes: a direct charge separation from the tolandiamine excited-state yielding **A**$^{-}$**-Tara1-Tara2-(Tara3)**$^{+}$ (which occurs in 200−300 fs) and a slower *indirect* hole transfer from the CT state **A**$^{-}$**-(Tara1)**$^{+}$**-Tara2-Tara3** to **A**$^{-}$**-Tara1-Tara2-(Tara3)**$^{+}$ in 20 ps (see Figure 12). The latter process is analogous to the ones observed in the shorter cascades. In **4** there are actually two similar but distinctly different tolandiamine groups which should result in (partially) overlapping absorption transitions. Nevertheless, these two tolandiamine units are likely to exhibit different reactivity with respect to hole transfer. The direct charge separation process can be rationalized based on the fact that the tetraaryl tolandiamine adjacent to the acridine is actually an electron D/A moiety which can form biradical intermediates. Hence, upon excitation of the tolandiamine system in **4** there

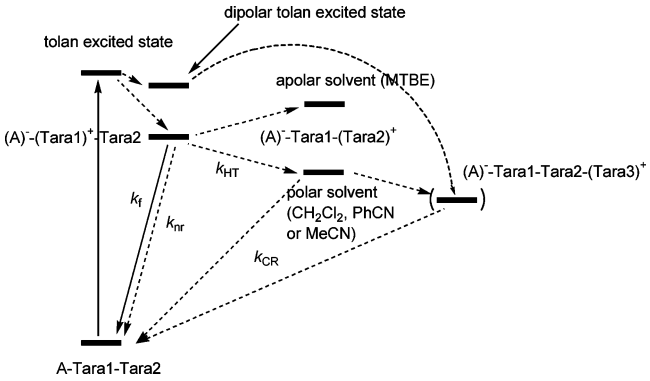

Figure 12. State diagram for **1**, **2**, and **5** (left-hand side) and for **4** (extension right-hand side).

Table 7. Rise Time τ_{HT} of the TA Peak at Ca. 740 nm and k_{HT} as Well as Life Time τ_{CR} of the Final Charge Separated State and k_{CR} of the Charge Recombination.

	acetonitrile (TA)		benzonitrile(TA)		CH_2Cl_2
	τ_{HT}/ps (k_{HT}/10^9 s^{-1})	τ_{CR}/ps (k_{CR}/10^9 s^{-1})	τ_{HT} /ps (k_{HT} /10^9 s^{-1})	τ_{CR}/ps (k_{CR}/10^9 s^{-1})	(fluoresc.) (k_{HT}/10^9 s^{-1})
1	3.2 (310)	22 (45)	30 (33)	180 (5.5)	(1.2)
4	20 (50)	410 (2.5)	250 (4)	>2000 (<0.5)	(0.20)
5	2.3 (440)	23 (44)	28 (36)	480 (2.1)	(0.96)

is—dependent on the conformation of the molecule—an initial extent of charge separation which will immediately undergo relaxation toward the final extended charge transfer state within 200−300 fs.

The rate constants for HT and charge recombination resulting from spectra deconvolution of the pump−probe measurements for **1**, **2**, **4**, and **5** in acetonitrile and benzonitrile are collected in Table 7. From these data it is apparent that the extension of the cascade (**4** vs **1**) slows down both k_{HT} and k_{CR} by one order of magnitude. In the same way, replacement of the polar acetonitrile by the less polar benzonitrile slows down both rate constants by one order of magnitude because back electron transfer occurs in the Marcus inverted region. For comparison, the rate constants k_{HT} from fluorescence measurements in CH_2Cl_2 are also given in Table 7. The values are still smaller than those obtained in benzonitrile because CH_2Cl_2 is somewhat less polar than benzonitrile.

Conclusions

From the fluorescence data in Table 6 it is obvious that the hole transfer from **Tara1** to **Tara2** is rapid and is the same for **1**, **2** and **5** in CH_2Cl_2 within experimental error. The hole transfer can compete very efficiently with the deactivation pathways in the reference chromophores as can be seen from the fluorescence quantum yields which are very low for **1**, **2**, **4**, and **5** (0.01−0.02 in CH_2Cl_2) but high for the reference compounds **6** and **7** (0.90 and 0.58, respectively, in CH_2Cl_2). Interestingly, there is no significant difference for the hole transfer rate in the branched molecule **5** compared to the linear array **1**. However, the hole transfer from **Tara1** to **Tara2** in **4** is significantly slower because of the lower free energy difference between **Tara2** and **Tara1** in **4** compared to that in e.g. **1** due to the methyl substitution in **Tara2** of **4**. This conclusion is fully supported by the pump−probe measurements in acetonitrile and benzonitrile. The hole transfer in **1**, **2**, **4**, and **5** should lead to a charge separation, i.e., a negative charge on acridine (**A**), and a positive

charge on **Tara2**. In the case of **4** one can expect that the smaller redox potential of **Tara3** compared to **Tara2** leads to a second hole transfer step in which the hole migrates to the terminal **Tara3**. If less polar solvents than CH_2Cl_2 are used, hole transfer in **1**, **2**, **4**, and **5** is either too slow or even unfavorable because the free energy difference of charge separation is very sensitive to the polarity of the solvent. In the case of **3**, the hole transfer is unfavorable irrespective of the solvent due to the wrong direction of the redox gradient.

The temporal evolution of the fs-broadband pump−probe spectra provides detailed insight into the photophysical properties of **1**−**8**, e.g., the data show that the extent of charge separation in the CT state of **8** strongly depends on the solvent. While in acetonitrile rapid energy localization competes with photoinduced charge transfer in benzonitrile these processes are distinctly separated on the time scale, the latter process being absent in MTBE.

The analysis of the TA spectra of **1** and **3** prove the HT process of **1** in polar solvents along the redox gradient while this process is uphill in **3**. The TA spectra also reveal the close analogy of the branched **5** to the single cascade **1**. For the extended cascade **4** the TA spectra suggest that two different processes lead to the final charge separated state, a direct charge separation which follows the excitation of the tolandiamine antenna moieties and a much slower process which involves the generation of a CT state followed by a HT step analogous to those in **1** and **5**. In the compounds **1**, **2** and **5** but especially in **4** the tolandiamine moieties not only serve as the cascade backbone but also possess a distinct antenna effect which collects all primary excitation energy.

In conclusion, we were able to show that acridine-triarylamine redox cascades can be used in efficient photoinduced electron-transfer processes. This PET can be governed by fine-tuning of the local redox potentials of the triarylamine redox centers, i.e., the redox gradient along the cascade molecules. Close analogy to triarylamine compounds used in optoelectronic devices make the presented arrays hopeful candidates for applications in, e.g., solar cells or photoconductors.

Experimental Section

Cyclic Voltammetry. The electrochemical experiments have been performed using a conventional three-electrode setup with a platinum disk working electrode in dry, argon-saturated CH_2Cl_2 with 0.2 M tetrabutylammonium hexafluorophosphate (TBAH) as supporting electrolyte and 0.001 M substrate. The potentials are referenced against ferrocene (Fc/Fc^+). The reversibility or irreversibility, respectively, of all redox processes were checked by measurements at different scan rates.

UV−vis/NIR and Fluorescence Spectroscopy. The UV−vis/NIR spectra were recorded with a JASCO V570 spectrometer in transmission. Steady-state fluorescence spectra were recorded with a PTI QuantaMaster Model QM-2000-4 spectrometer using degassed, argon saturated solvents in the μM concentration range. The spectra are corrected for the wavelength sensitivity of the detector. Spectra are converted to wavenumber scale by multiplication of the intensity with λ^2. Fluorescence quantum yields were determined relative to rhodamine 101 in EtOH (conc = ca. 1 μM) which has a quantum yield of 1.00. The quantum yields are corrected for the index of refraction of the solvent. Fluorescence decays were measured with a PTI TimeMaster Model TM-2/2003 stroboscopic boxcar spectrometer and a flash lamp charged with a H_2/N_2 1:1 mixture. Excitation wavelength was 381 nm for all compounds. The instrument response function was obtained by using a dilute coffee creamer as a scatterer. The decay fits were single exponential in all cases as checked by the χ^2 value, the Durbin−Watson parameter and the final residuals.

Femtosecond Broadband Pump−Probe Setup. A detailed description of the setup has been been given elsewhere.[58] Briefly, the compounds were exited by pump pulses at 360 nm at $5 \times 10^{-4} - 5 \times 10^{-6}$ M sample concentration. The changes in optical density were probed by a femtosecond white-light continuum (WLC) generated by tight focusing of a small fraction of the output of a commercial Ti:Sapphire based pump laser (CPA-2001, Clark-MXR) into a 3 mm CaF_2 plate. The obtained WLC provided a usable probe source between 370 and 720 nm. The WLC was split into two beams (probe and reference) and focused into the sample using reflective optics. After passing through the sample both probe and reference were spectrally dispersed and simultaneously detected on a CCD sensor. The pump pulse (340 nm, 100−200 nJ) was generated by frequency doubling of the compressed output of a commercial NOPA system (Clark-MXR, 680 nm, 8 μJ, 30 fs). To compensate for group velocity dispersion in the UV-pulse we used an additional prism compressor. Independent measurements of the chirp of the WLC were carried out to correct the pump−probe spectra for time-zero differences. The overall time resolution of the setup was obtained from the rise time of the signal (above 580 nm). Assuming a Gaussian shape cross-correlation we obtained a width of 100−120 fs (fwhm). A spectral resolution of 7−10 nm was obtained. Measurements were performed with magic angle geometry (54.7°) for the polarization of pump and probe pulses to avoid contributions from orientational relaxation. Pump energy and pump spot size (~200−400 μm) were adjusted to minimize contributions from the solvent to the signal. Steady-state absorption and fluorescence spectra of the samples measured before and after the time-resolved experiments were compared with each other and no indications for degradation were found. A sample cell with 1.25 mm fused silica windows and a light path of 1 mm was used for all measurements. No indications for aggregation could be observed in the measurements.

Acknowledgment. This work was supported by the Fonds der Chemischen Industrie, the Deutsche Forschungsgemeinschaft, the Volkswagenstiftung, and the Bayerisches Staatsministerium für Wissenschaft, Forschung und Kunst (FORMAT project). We thank JASCO GmbH Deutschland as well as Heraeus GmbH for kind support.

Note Added after ASAP Publication. After this article was published ASAP on July 7, 2005, a production error in the redox potential difference equation for **1** in the text just above eq 5 was discovered. The corrected version was published ASAP on July 11, 2005.

Supporting Information Available: Synthetic details and characterization for all compounds. X-ray crystallographic analysis data for **8**. This material is available free of charge via the Internet at http://pubs.acs.org.

JA0511570

(58) Raytchev, M.; Pandurski, E.; Buchvarov, I.; Modrakowski, C.; Fiebig, T. *J. Phys. Chem. A* **2003**, *107*, 4592−4600.